Supporting Information

A new quinoline-based fluorescent probe for Cd^{2+} and Hg^{2+} with an opposite response in 100% aqueous environment and living cell imaging

Hong-Lin Lu,[a] Wei-Kang Wang,[b] Xing-Xing Tan,[a] Xiao-Fei Luo,[a] Mao-Lin Zhang,[a] Mei Zhang[a,*] and Shuang-Quan Zang[a,*]

[a] *College of Chemistry and Molecular Engineering, Zhengzhou University, Zhengzhou 450001, China*

[b] *Basic Medical College, Zhengzhou University, Zhengzhou 450001, China*

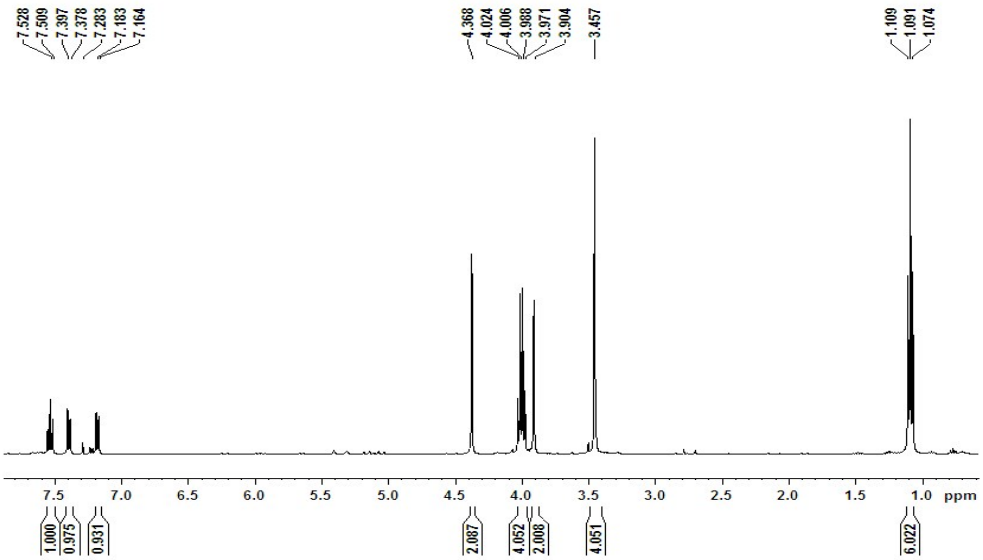

Fig. S1. ^{1}H NMR spectrum of compound **1** in $CDCl_3$.

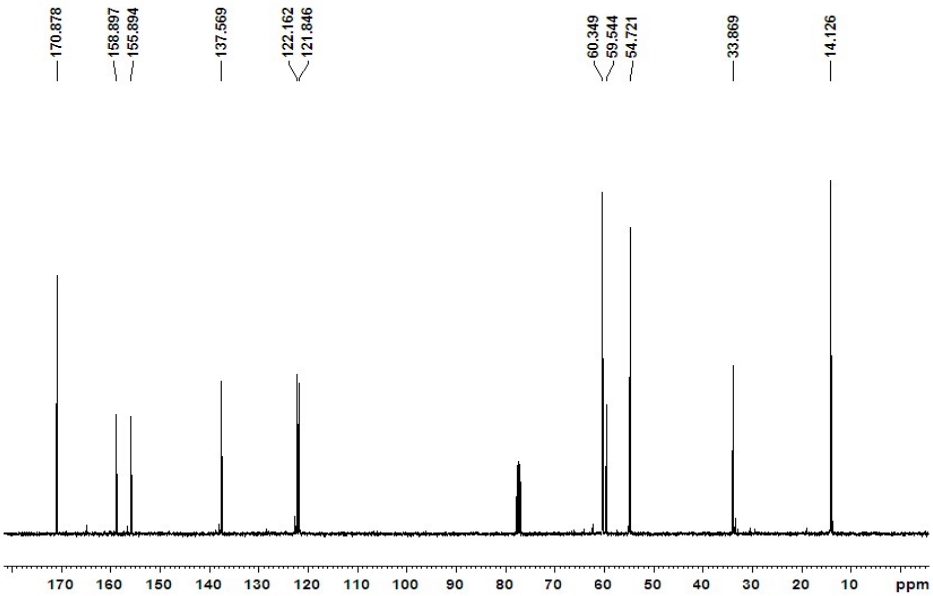

Fig. S2. ^{13}C NMR spectrum of compound **1** in $CDCl_3$.

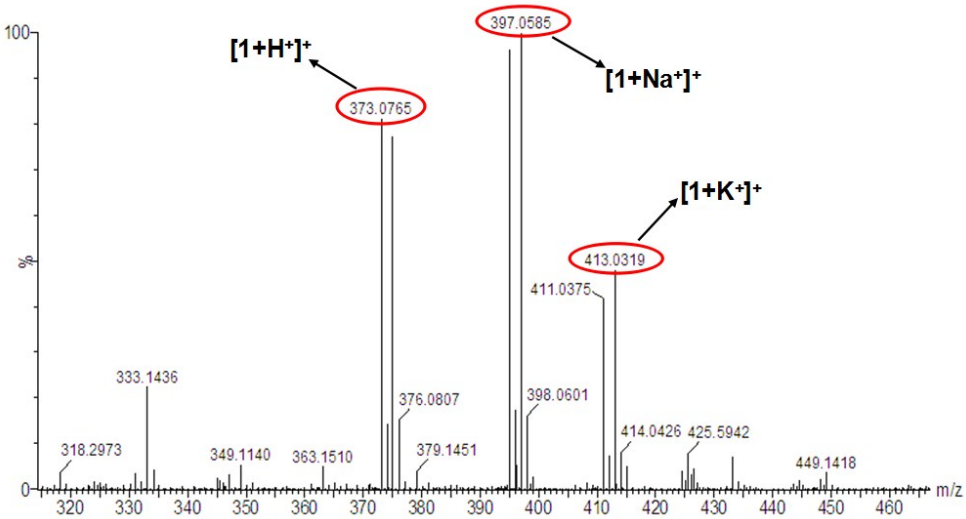

Fig. S3. ESI-MS spectrum of compound **1** in methanol.

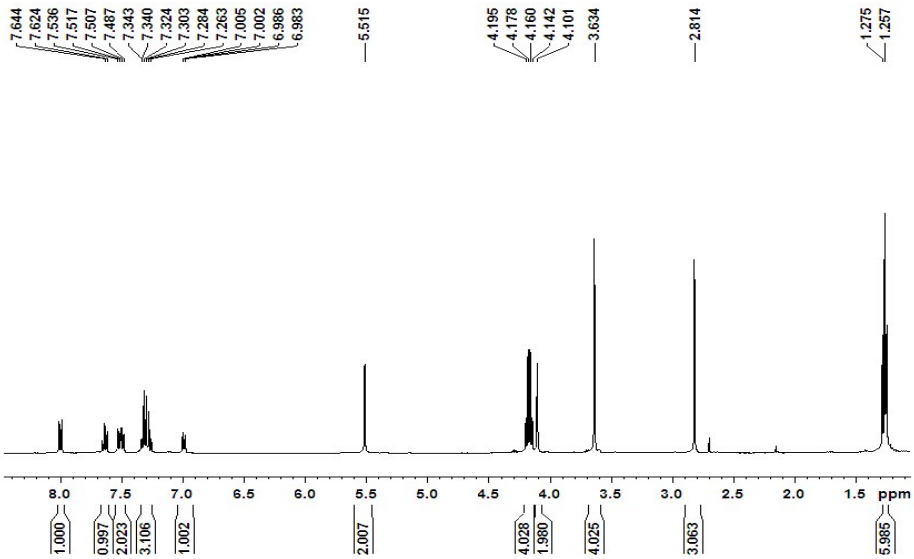

Fig. S4. ^{1}H NMR spectrum of **L** in $CDCl_3$.

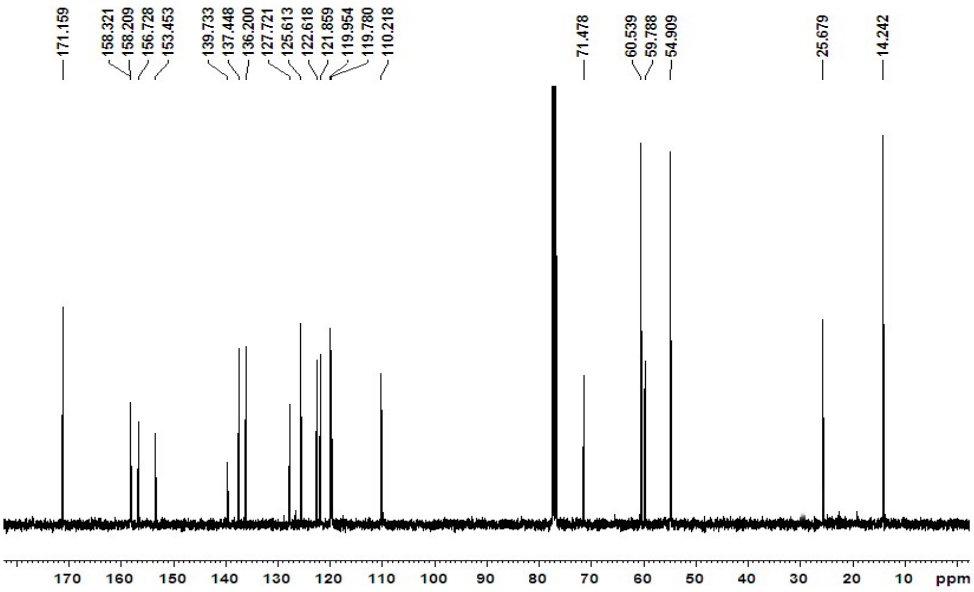

Fig. S5. ^{13}C NMR spectrum of **L** in $CDCl_3$.

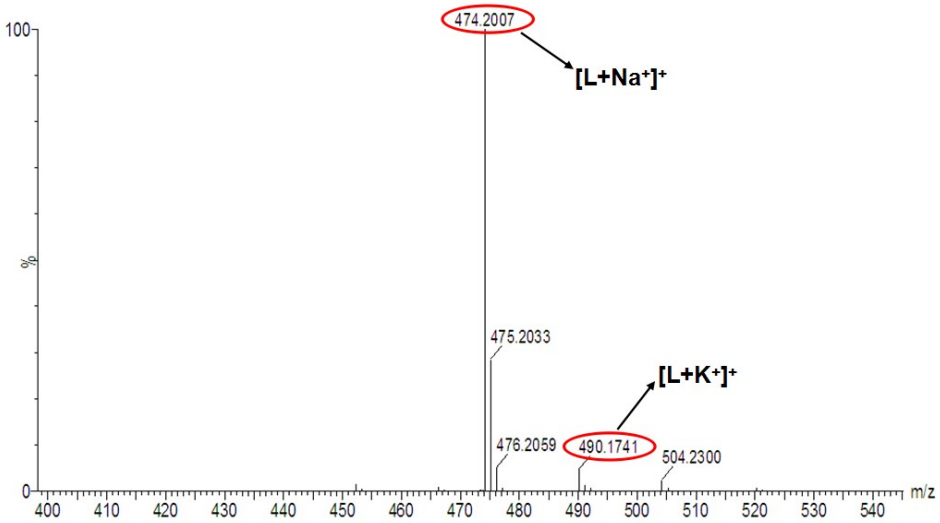

Fig. S6. ESI-MS spectrum of **L** in methanol.

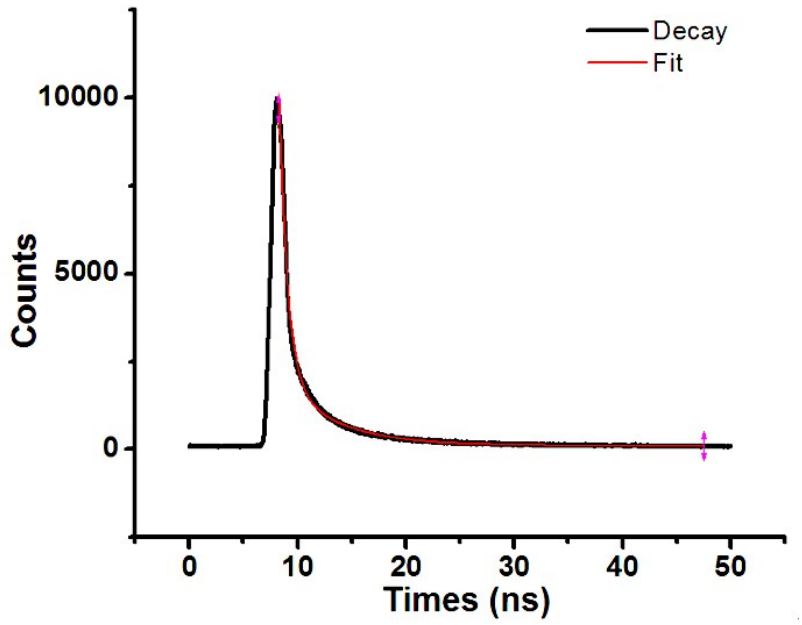

Fig. S7. Fluorescence decay curve of **L** at 415 nm in aqueous solution (λ_{ex} = 243 nm).

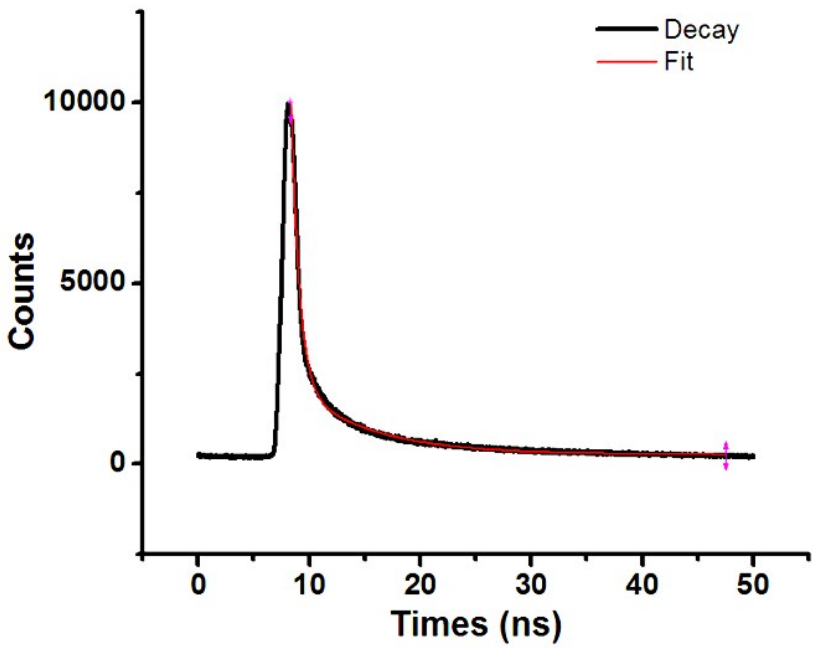

Fig. S8. Fluorescence decay curve of **L** at 415 nm in the presence of 10 equiv Cd^{2+} in aqueous solution (λ_{ex} = 243 nm).

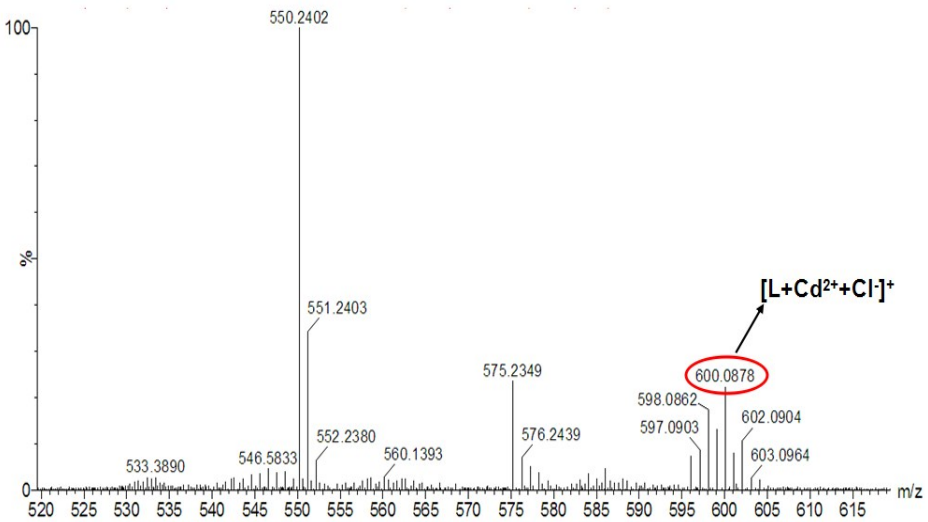

Fig. S9. ESI-MS spectrum of **L** in the presence of $CdCl_2$ in methanol.

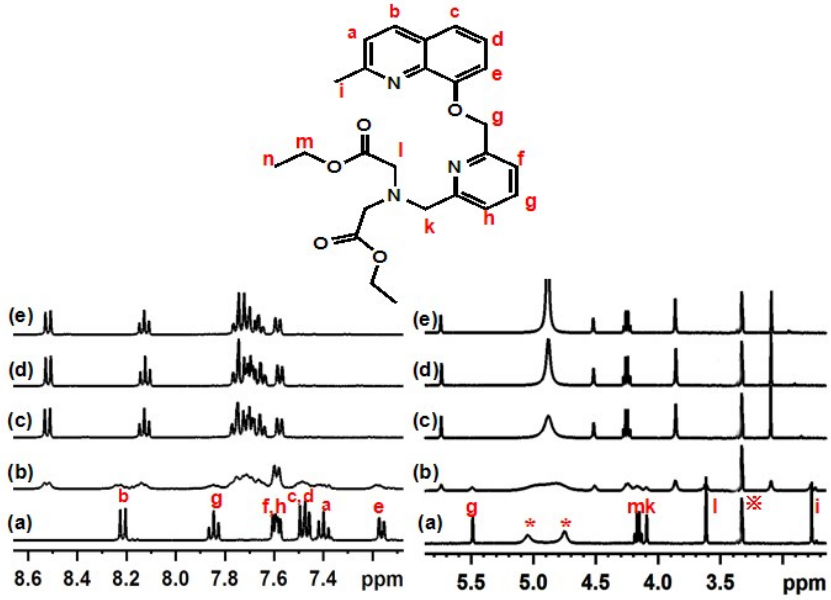

Fig. S10. ^{1}H NMR (400 MHz) spectral changes of **L** in CD_3OD/D_2O (4:1) upon addition of $CdCl_2$ at 298 K. (a) **L**, (b) **L** + Cd^{2+} (1:0.5), (c) **L** + Cd^{2+} (1:1), (d) **L** + Cd^{2+} (1:2), (e) **L** + Cd^{2+} (1:5), where ∗ denotes the residual proton signal from D_2O and ※ denotes the residual proton signal from CD_3OD.

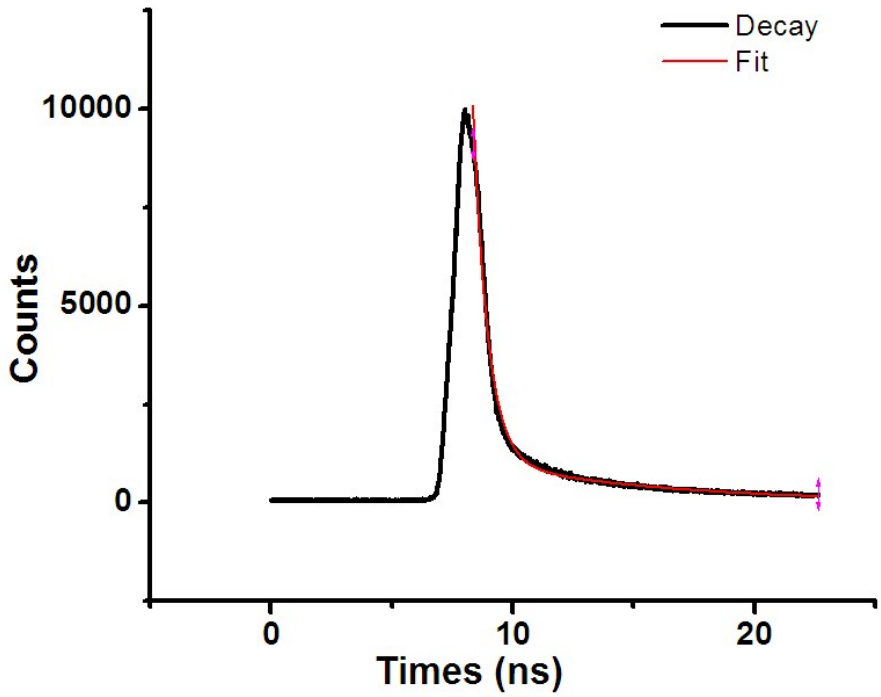

Fig. S11. Fluorescence decay curve of **L** at 415 nm in the presence of 10 equiv Hg^{2+} in aqueous solution (λ_{ex} = 243 nm).

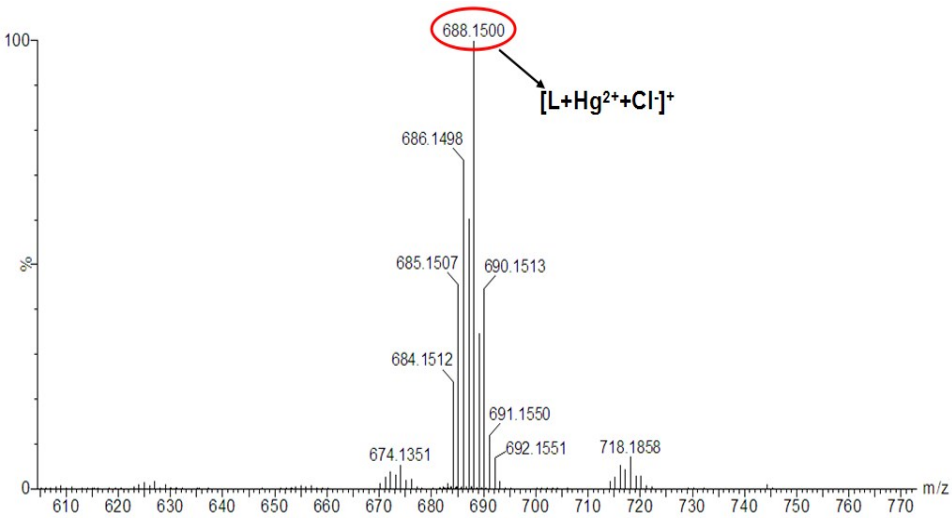

Fig. S12. ESI-MS spectrum of **L** in the presence of $HgCl_2$ in methanol.

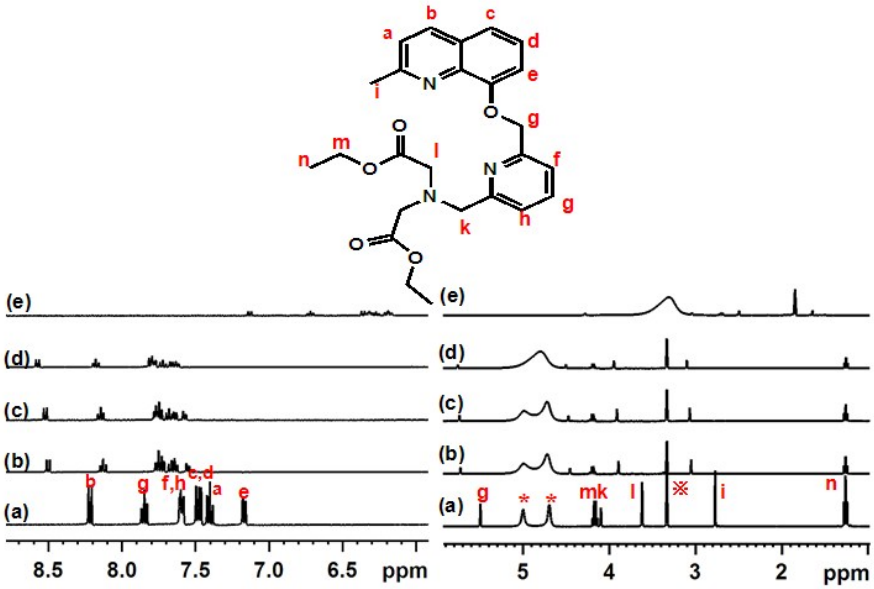

Fig. S13. ^{1}H NMR (400 MHz) spectral changes of **L** in CD_3OD/D_2O (4:1) upon addition of $HgCl_2$ at 298 K. (a) **L**, (b) **L** + Hg^{2+} (1:0.5), (c) **L** + Hg^{2+} (1:1), (d) **L** + Hg^{2+} (1:2), (e) **L** + Hg^{2+} (1:5), where ∗ denotes the residual proton signal from D_2O and ※ denotes the residual proton signal from CD_3OD.

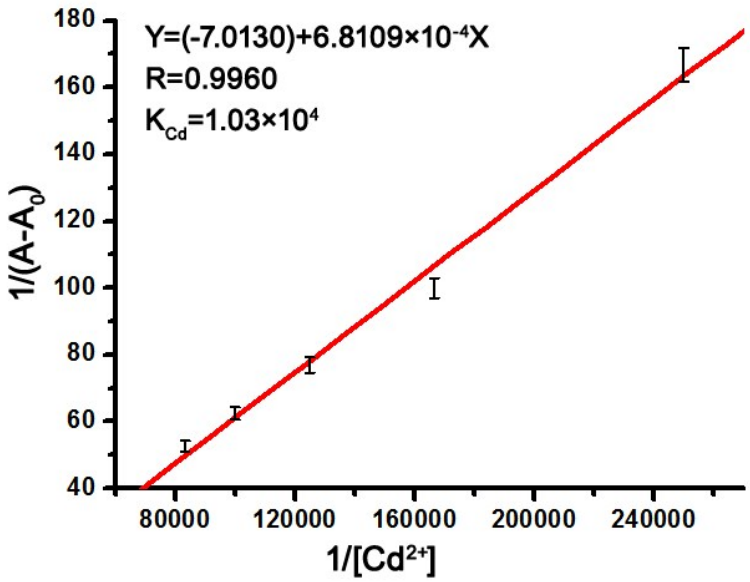

Fig. S14. Benesi–Hildebrand plot of **L** (10 μM) assuming 1:1 stoichiometry between **L** and Cd^{2+} in aqueous solution. The binding constant of **L**-Cd^{2+} was 1.03×10^4 M^{-1}.

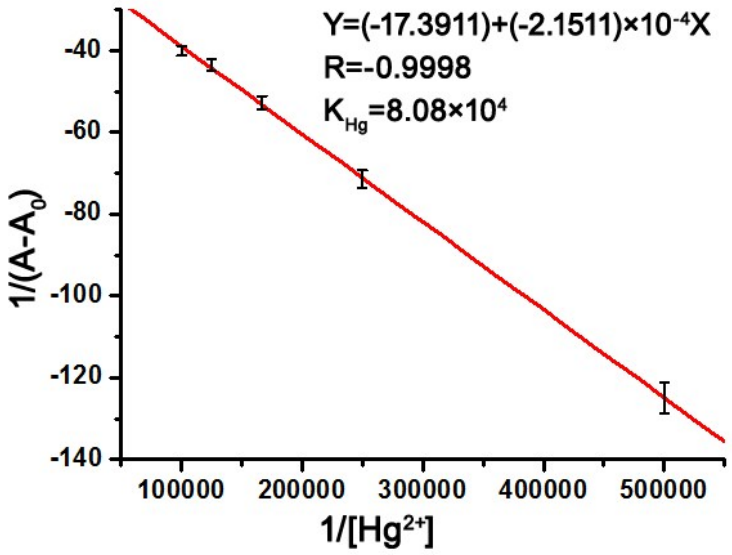

Fig. S15. Benesi–Hildebrand plot of **L** (10 μM) assuming 1:1 stoichiometry between **L** and Hg^{2+} in aqueous solution. The binding constant of **L**-Hg^{2+} was 8.08×10^4 M^{-1}.

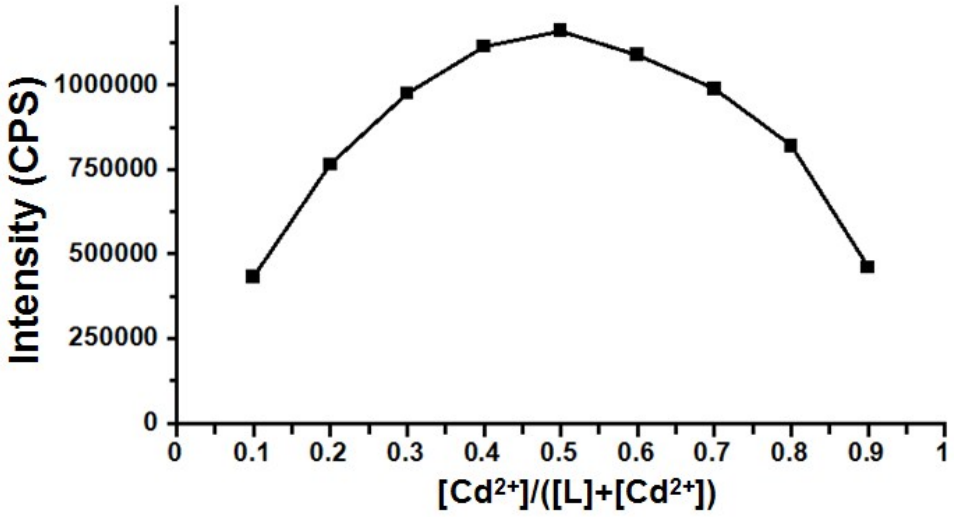

Fig. S16. Job's plot for **L** with Cd^{2+} in aqueous solution measured at 415 nm.

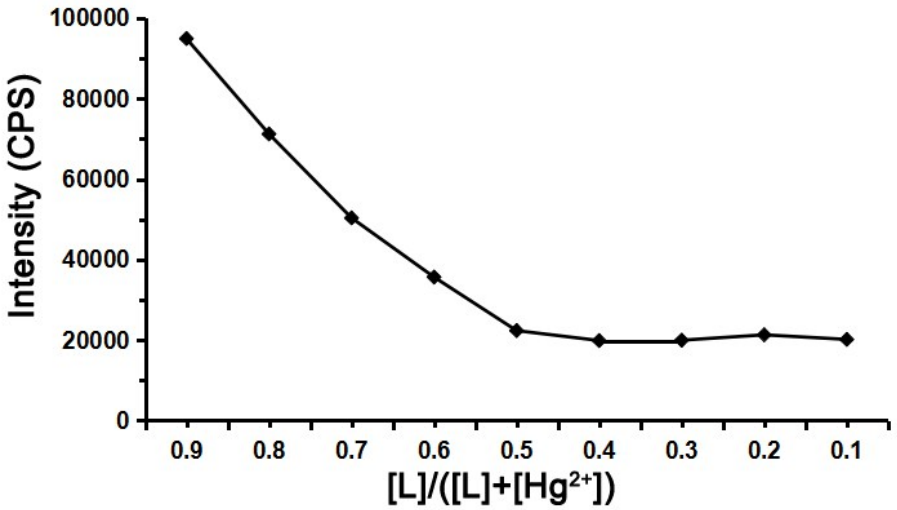

Fig. S17. Job's plot for **L** with Hg^{2+} in aqueous solution measured at 415 nm.

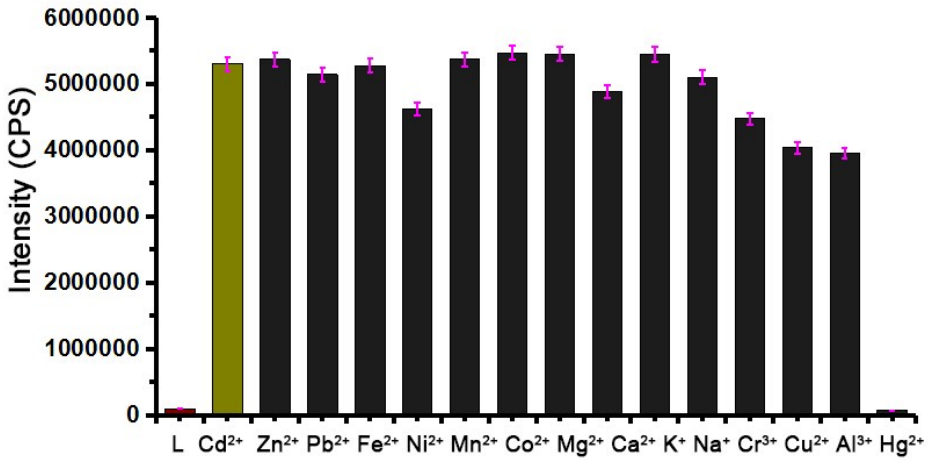

Fig. S18. Fluorescence responses (λ_{ex} = 243 nm) of **L** (10 μM) at 415 nm in aqueous solutions. Brick-red bar: a free probe. Olive bar: a probe (10 μM) treated with 10 equiv Cd^{2+}. Black bars: a probe (10 μM) treated with the marked metal ions (10 equiv) followed by 10 equiv of Cd^{2+}.

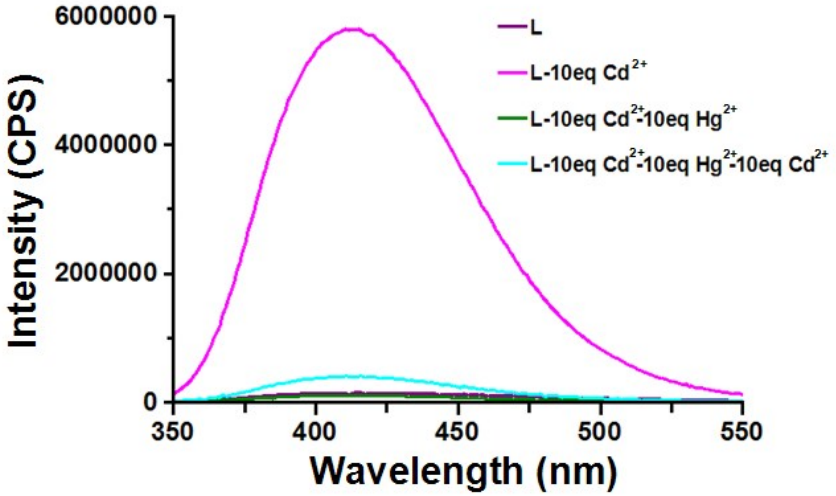

Fig. S19. Fluorescence spectra of **L** (10 μM) upon titrating different molar ratio of Cd^{2+} and Hg^{2+}: 10 equiv. Cd^{2+} (First) + 10 equiv. Hg^{2+} (Second) + 10 equiv. Cd^{2+} (Third) in aqueous solutions. The excitation wavelength was 243 nm.

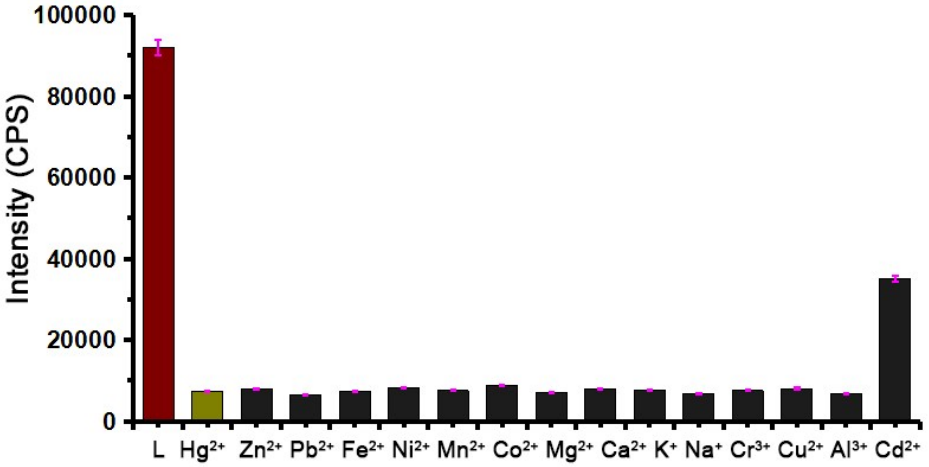

Fig. S20. Fluorescence responses (λ_{ex} = 243 nm) of **L** (10 μM) at 415 nm in aqueous solutions. Brick-red bar: a free probe. Olive bar: a probe (10 μM) treated with 10 equiv Hg^{2+}. Black bars: a probe (10 μM) treated with the marked metal ions (10 equiv) followed by 10 equiv of Hg^{2+}.

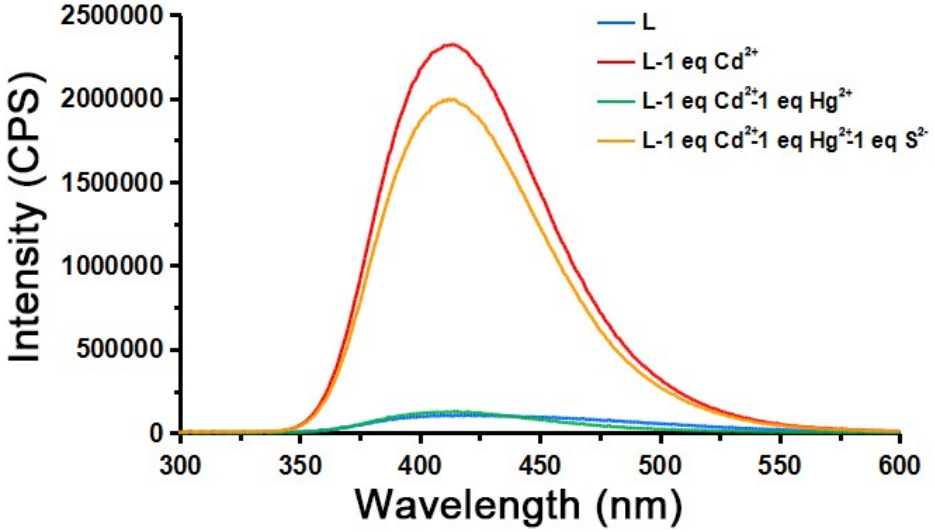

Fig. S21. Fluorescence spectral changes of **L** (10 μM) at 415 nm treated with 1 eqv. Cd^{2+} (red line), 1 eqv. Hg^{2+} (green line) and 1 eqv. S^{2-} (orange line).

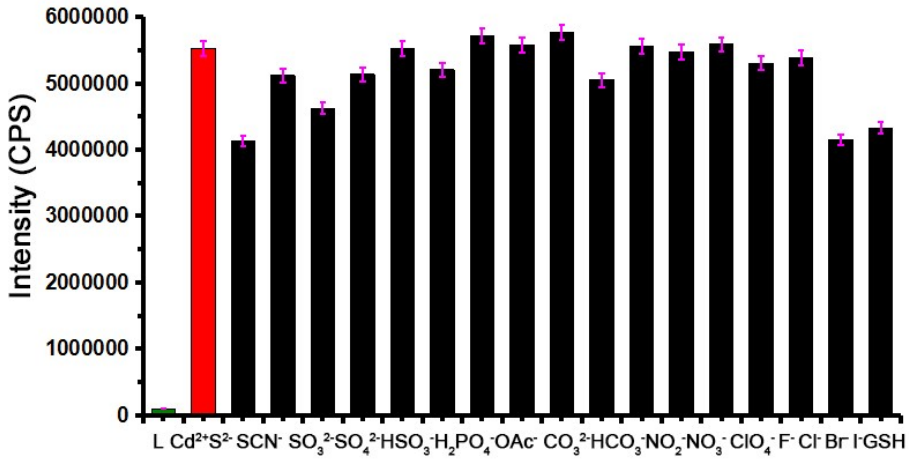

Fig. S22. Fluorescence responses (λ_{ex} = 243 nm) of **L** (10 μM) at 415 nm treated with marked anions (10 equiv) followed by 10 equiv Cd^{2+} in aqueous solutions. Green bar: a free probe (10 μM). Red bar: a probe (10 μM) treated with Cd^{2+} (10 equiv). Black bars: a probe (10 μM) treated with the marked anions and GSH (10 equiv) followed by 10 equiv of Cd^{2+}.

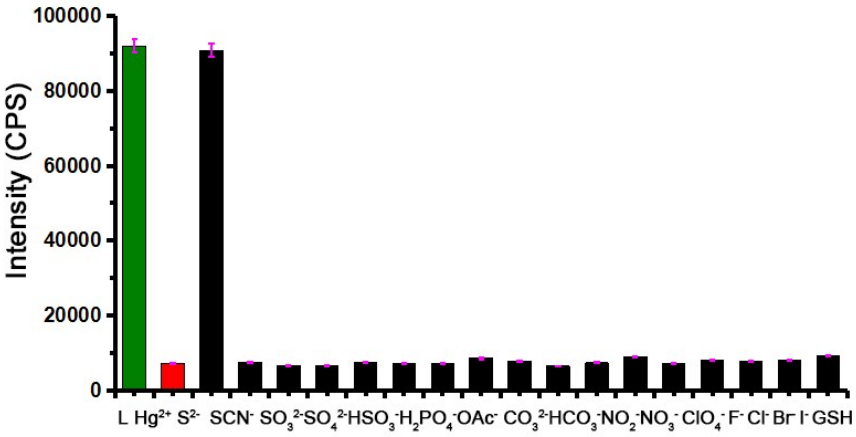

Fig. S23. Fluorescence responses (λ_{ex} = 243 nm) of **L** (10 μM) at 415 nm treated with marked anions (10 equiv) followed by 10 equiv Hg^{2+} in aqueous solutions. Green bar: a free probe (10 μM). Red bar: a probe (10 μM) treated with Hg^{2+} (10 equiv). Black bars: a probe (10 μM) treated with the marked anions and GSH (10 equiv) followed by 10 equiv of Hg^{2+}.

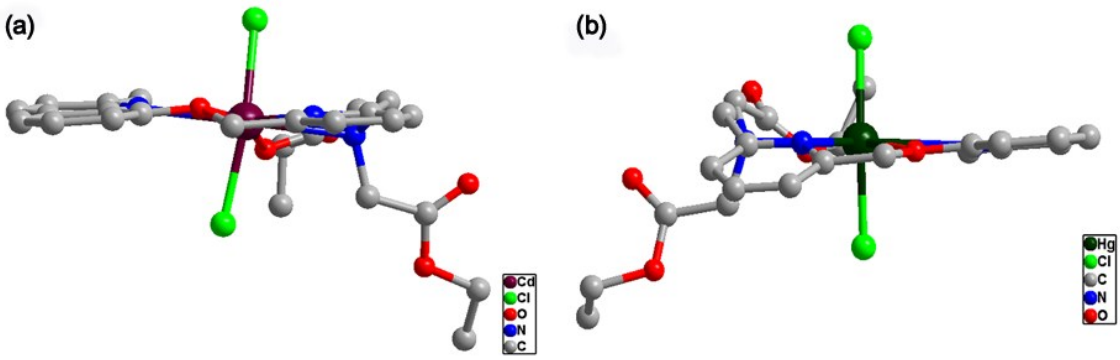

Fig. S24. Crystal structures of **L**-Cd^{2+} complex (a) and **L**-Hg^{2+} complex (b). All hydrogen atoms were omitted for clarify.

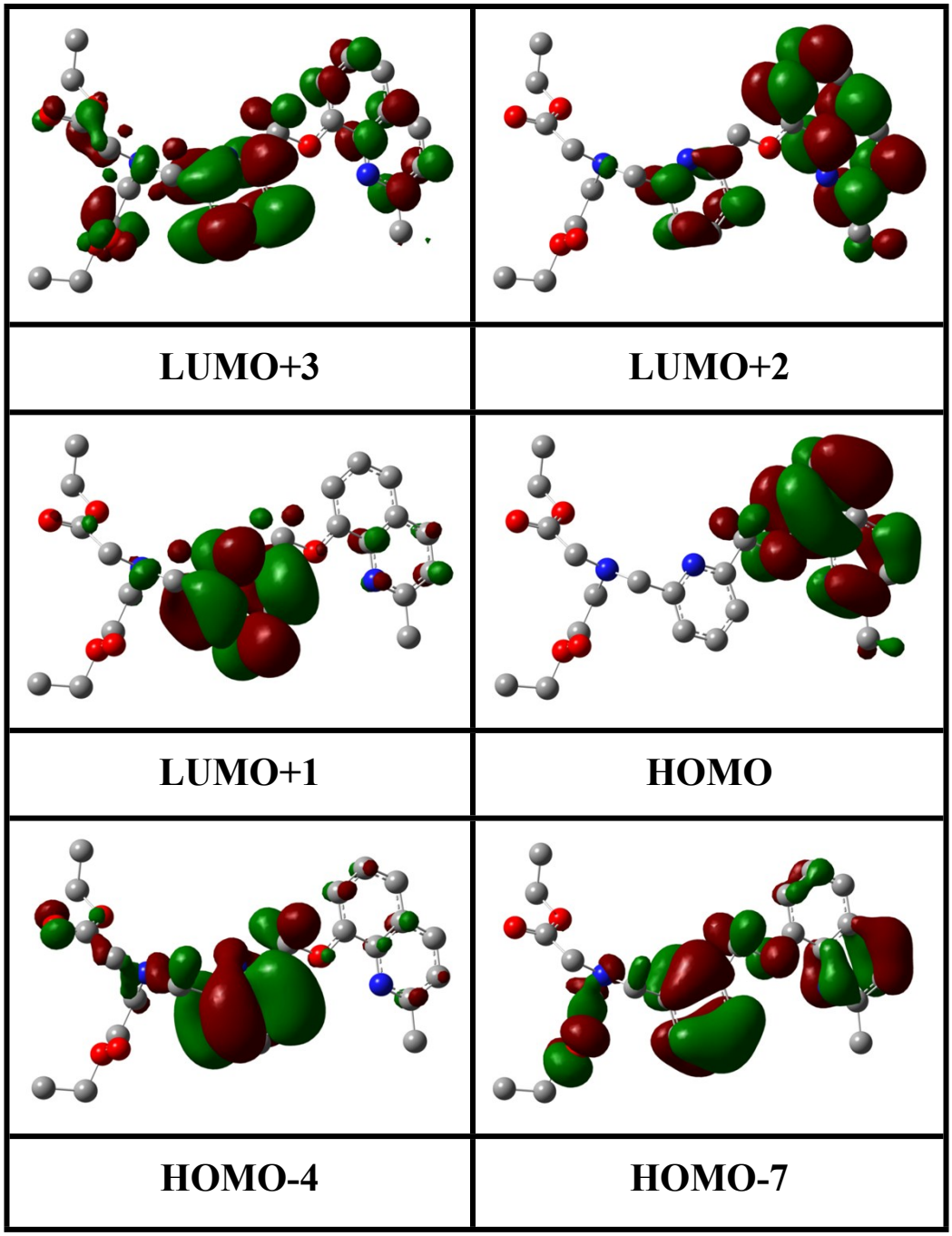

Fig. S25. Frontier molecular orbitals of **L**.

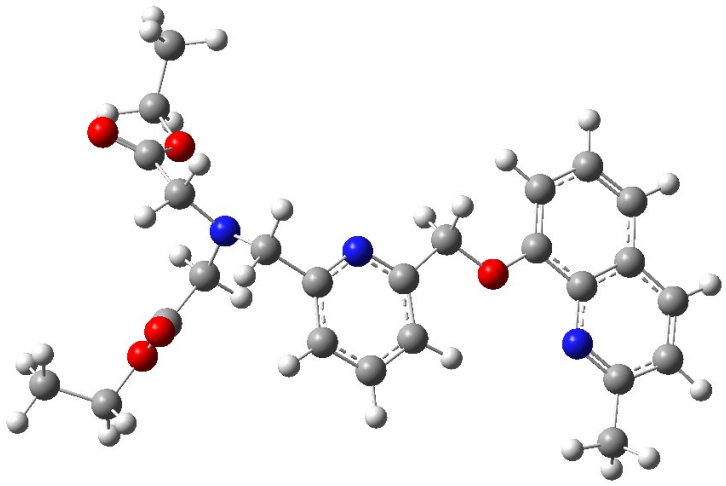

Fig. S26. DFT optimized structures of **L**.

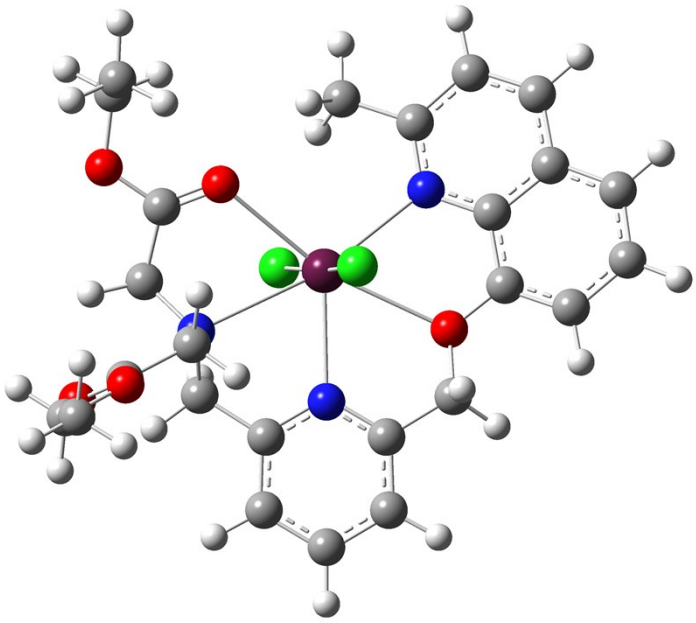

Fig. S27. DFT optimized structures of complex **L**-Cd^{2+}.

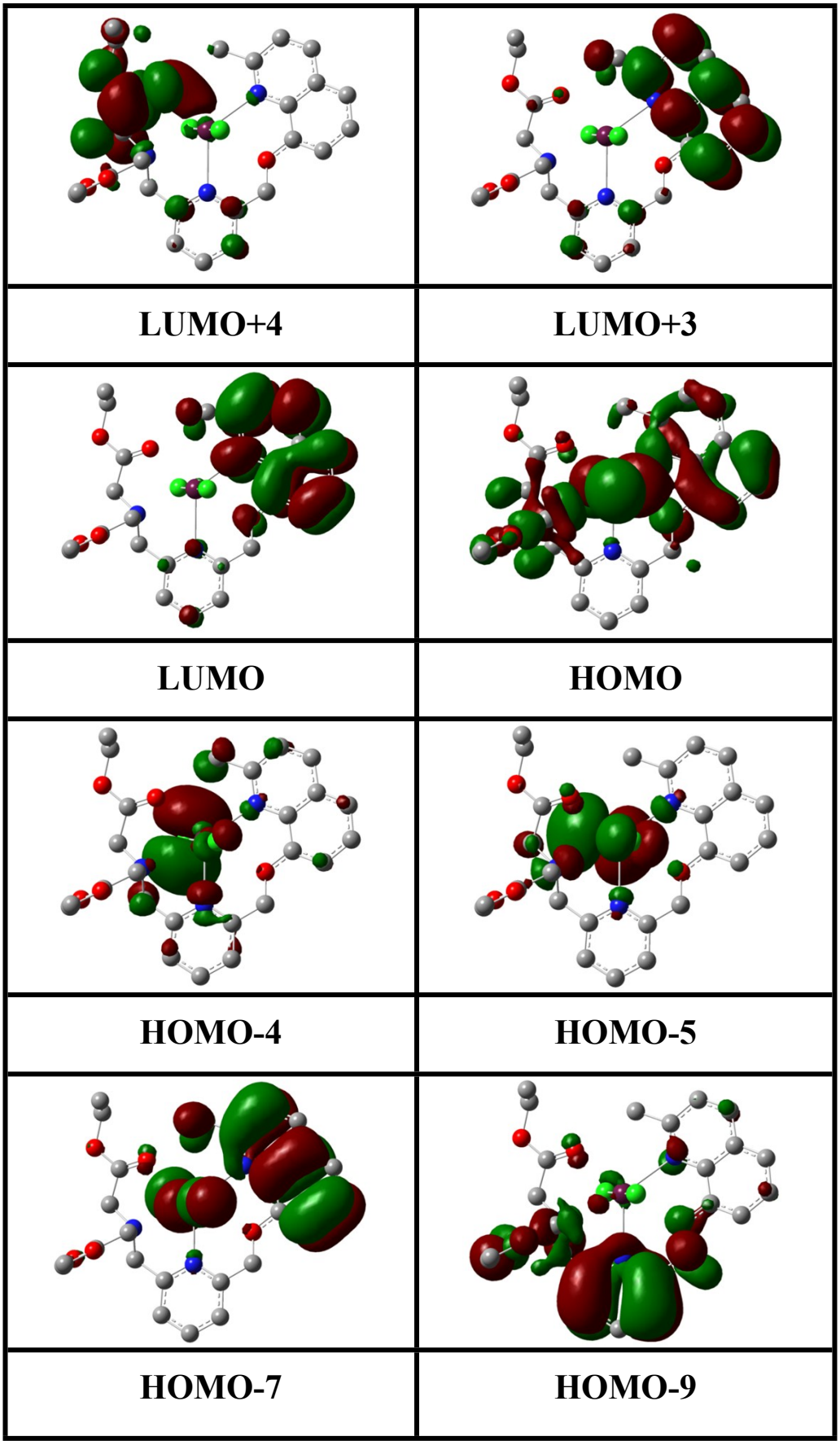

Fig. S28. Frontier molecular orbitals of **L**-Cd^{2+}.

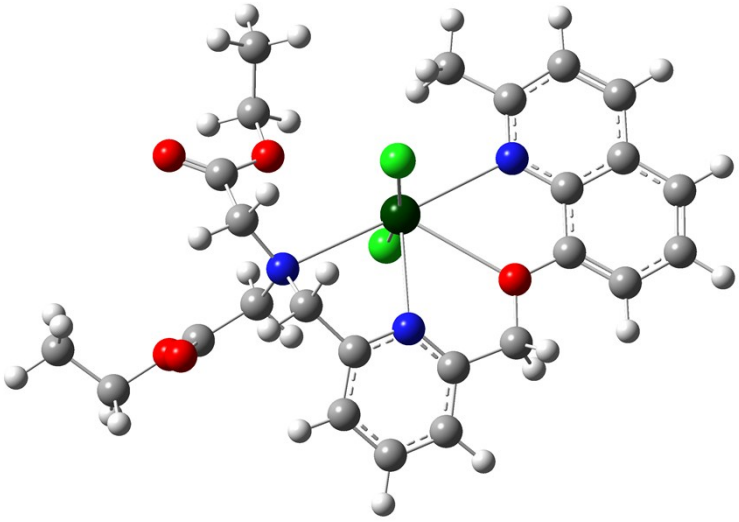

Fig. S29. DFT optimized structures of complex **L**-Hg^{2+}.

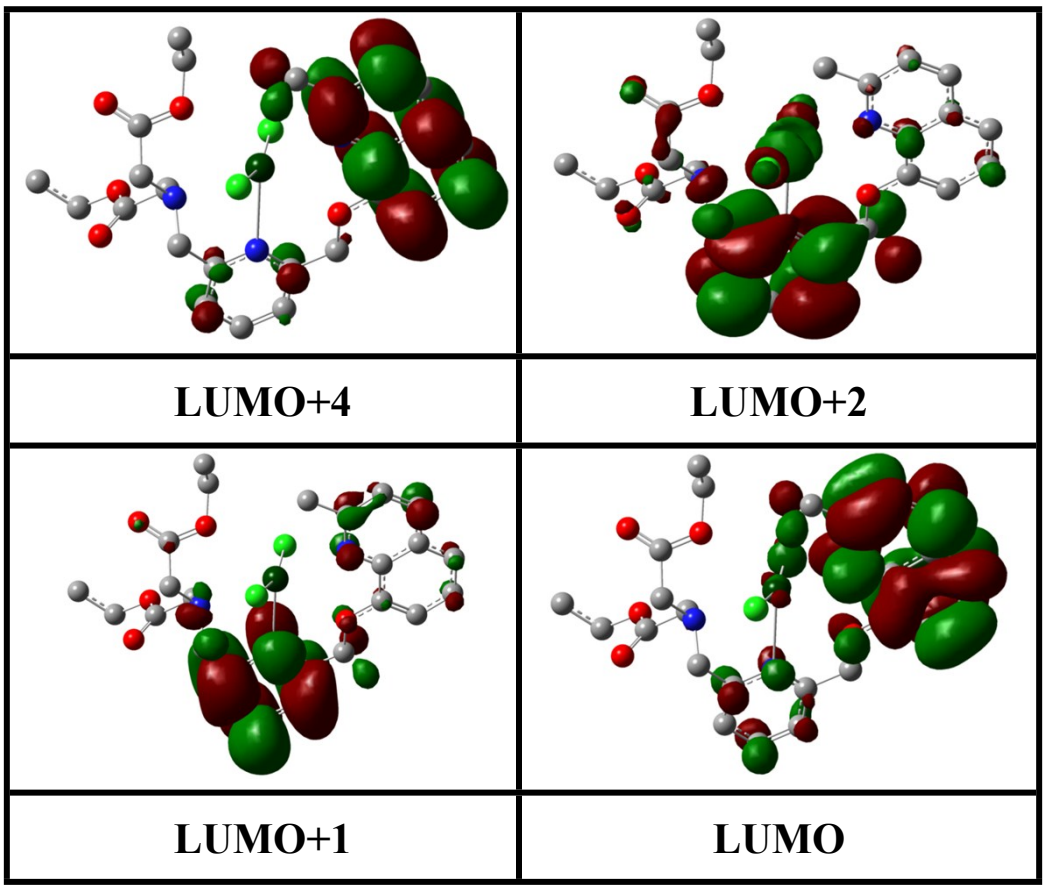

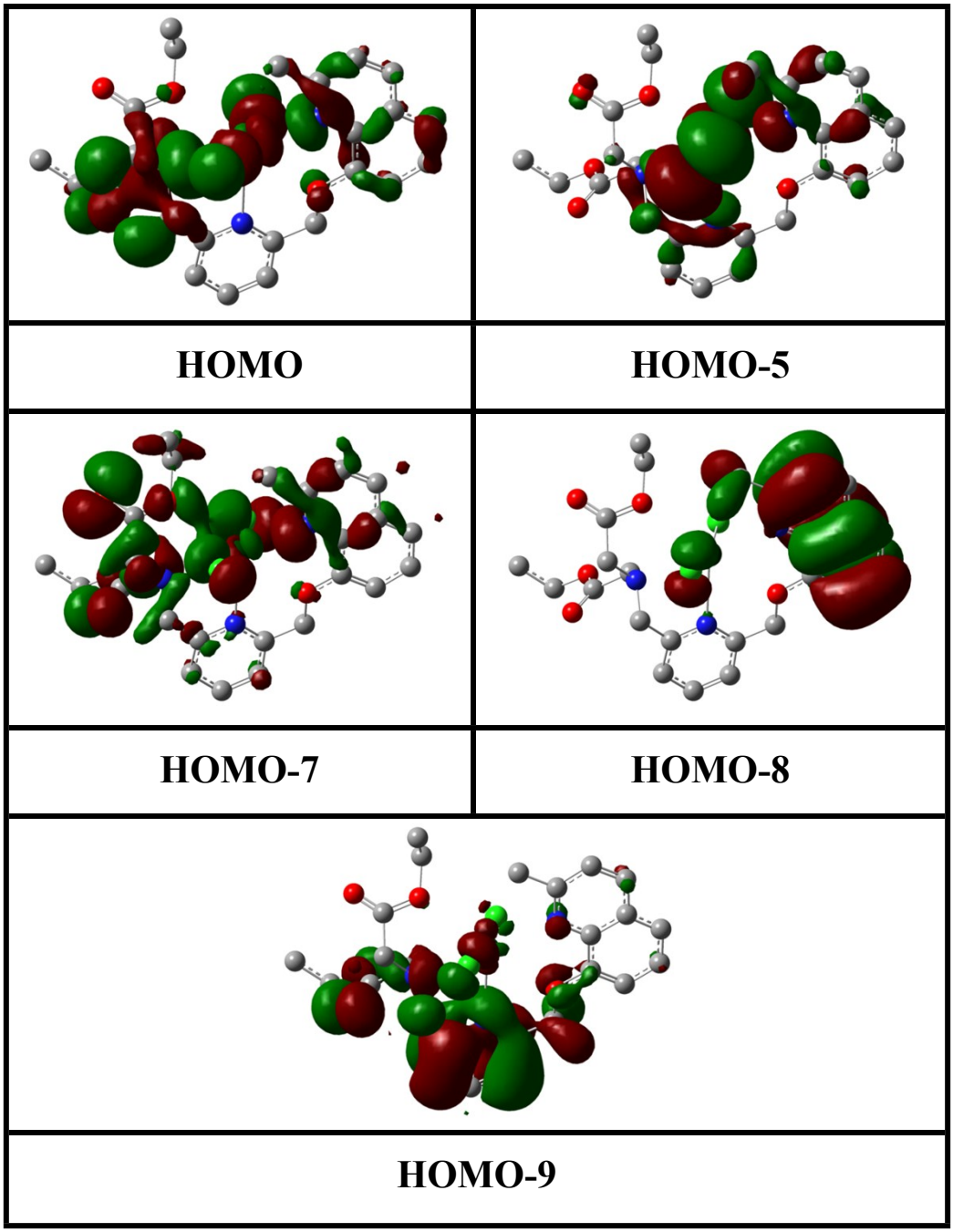

Fig. S30. Frontier molecular orbitals of **L**-Hg^{2+}.

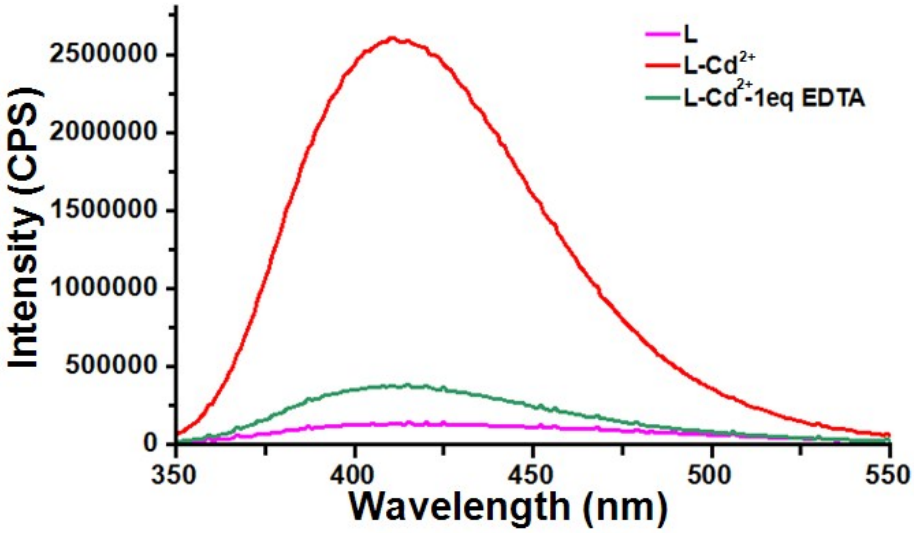

Fig. S31. Reversibility of Cd^{2+} (10 μM) coordination to **L** (10 μM) by EDTA disodium (10 μM) in aqueous solution. The excitation wavelength was 243 nm.

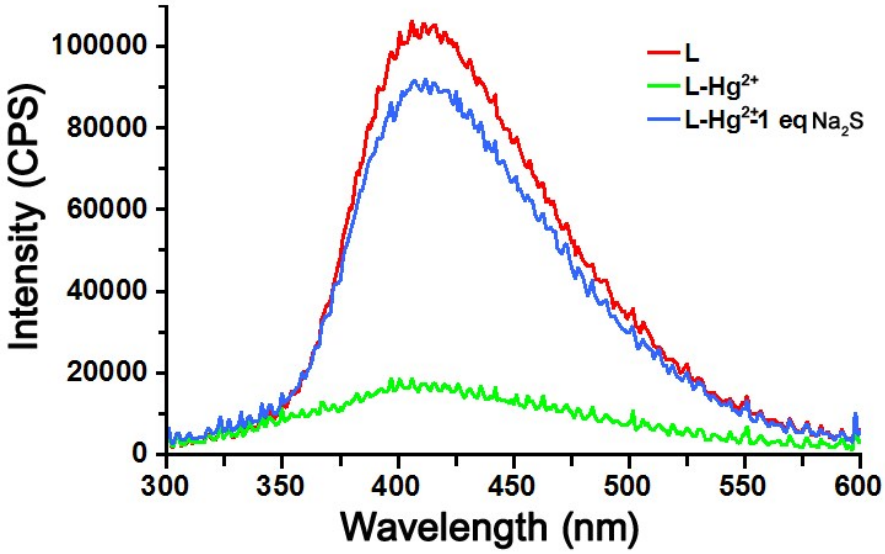

Fig. S32. Reversibility of Hg^{2+} (10 μM) coordination to **L** (10 μM) by Na_2S (10 μM) in aqueous solution. The excitation wavelength was 243 nm.

Table S1. Crystallographic data and structure refinement parameters for complex **L**-Cd^{2+}.

Compound	**L**-Cd^{2+}
Empirical formula	$C_{25}H_{29}CdCl_2N_3O_5$
Formula weight	634.82
Temperature (K)	293(2)
Crystal system	Monoclinic
Space group	*P21/c*
a (Å)	9.7380(3)
b (Å)	18.6367(5)
c (Å)	15.4077(5)
α (°)	90
β (°)	107.382(3)
γ (°)	90
V (Å^3)	2668.55(14)
Z	4
D_c (Mg/m^3)	1.580
μ (mm^{-1})	0.962
F(000)	1260
Reflns collected	10888
Independent reflns	4695
Completeness	99.9 %
R(int)	0.0322
Refinement method	Full-matrix least-squares on F^2
Data / restraints / parameters	4695 / 0 / 328
GOF on F^2	0.965
$^aR_1[I>2\sigma(I)]$, wR_2	0.0375, 0.0749
R_1[all data], wR_2	0.0567, 0.0818

$^aR_1=\Sigma||F_o| - |F_c||/\Sigma|F_o|$, $wR_2=[\Sigma[w(F_o^2 - F_c^2)^2]/\Sigma w(F_o^2)^2]^{1/2}$

Table S2. Crystallographic data and structure refinement parameters for complex **L**-Hg^{2+}.

Compound	**L**-Hg^{2+}
Empirical formula	$C_{25}H_{29}Cl_2HgN_3O_5$
Formula weight	723.00
Temperature (K)	293(2)
Crystal system	Monoclinic
Space group	*P21/c*
a (Å)	12.6620(3)
b (Å)	11.8788(2)
c (Å)	18.7193(4)
α (°)	90
β (°)	98.172(2)
γ (°)	90
V (Å^3)	2786.97(10)
Z	4
D_c (Mg/m^3)	1.723
μ (mm^{-1})	5.753
F(000)	1416
Reflns collected	26353
Independent reflns	4897
Completeness	99.8 %
R(int)	0.0432
Refinement method	Full-matrix least-squares on F^2
Data / restraints / parameters	4889 / 122 / 348
GOF on F^2	1.083
$^aR_1[I>2\sigma(I)]$, wR_2	0.0395, 0.0941
R_1[all data], wR_2	0.0558, 0.0999

$^aR_1=\Sigma||F_o| - |F_c||/\Sigma|F_o|$, $wR_2=[\Sigma[w(F_o^2 - F_c^2)^2]/\Sigma w(F_o^2)^2]^{1/2}$

Table S3. Selected bond lengths (Å) and angles [°] for complex **L**-Cd^{2+}.

bond lengths (Å)			
Cd(1)-N(2)	2.419(3)	Cd(1)-O(1)	2.527(2)
Cd(1)-Cl(2)	2.4703(10)	Cd(1)-N(3)	2.656(3)
Cd(1)-Cl(1)	2.4942(9)	Cd(1)O(2)	2.7543(66)
Cd(1)-N(1)	2.498(3)		
bond angles (°)			
N(2)-Cd(1)-Cl(2)	96.69(7)	N(2)-Cd(1)-Cl(1)	97.73(7)
Cl(2)-Cd(1)-Cl(1)	165.26(4)	N(2)-Cd(1)-N(1)	130.07(9)
Cl(2)-Cd(1)-N(1)	84.84(7)	Cl(1)-Cd(1)-N(1)	88.19(7)
N(2)-Cd(1)-O(1)	65.29(8)	Cl(2)-Cd(1)-O(1)	87.53(6)
Cl(1)-Cd(1)-O(1)	101.25(6)	N(1)-Cd(1)-O(1)	64.93(8)
N(2)-Cd(1)-N(3)	67.83(9)	Cl(2)-Cd(1)-N(3)	95.88(7)
Cl(1)-Cd(1)-N(3)	86.79(7)	N(1)-Cd(1)-N(3)	161.98(9)
O(1)-Cd(1)-N(3)	133.07(8)	O(2)-Cd(1)-N(2)	129.088(158)
C(11)-O(1)-Cd(1)	116.85(19)	C(20)-N(3)-Cd(1)	107.1(2)
C(18)-N(3)-Cd(1)	108.60(19)	C(17)-N(3)-Cd(1)	103.90(19)
C(12)-N(2)-Cd(1)	121.7(2)	C(16)-N(2)-Cd(1)	119.9(2)
C(2)-N(1)-Cd(1)	122.9(2)	C(10)-N(1)-Cd(1)	117.9(2)

Table S4. Selected bond lengths (Å) and angles [°] for complex **L**-Hg^{2+}.

bond lengths (Å)			
Hg(1)-Cl(2)	2.368(2)	Hg(1)-Cl(1)	2.3735(18)
Hg(1)-N(2)	2.555(5)	Hg(1)-N(1)	2.7123(58)
Hg(1)-N(3)	2.8031(76)	Hg(1)-O(1)	2.7145(37)
bond angles (°)			
Cl(2)-Hg(1)-Cl(1)	161.46(8)	Cl(2)-Hg(1)-N(2)	99.04(14)
Cl(1)-Hg(1)-N(2)	97.21(13)	N(2)-Hg(1)-N(2)	121.746(161)
N(2)-Hg(1)-O(1)	62.339(153)	N(2)-Hg(1)-N(3)	67.449(179)
N(1)-Hg(1)-Cl(1)	86.353(128)	N(1)-Hg(1)-Cl(2)	92.613(130)
N(1)-Hg(1)-O(1)	59.438(144)	N(1)-Hg(1)-N(3)	170.548(184)
N(3)-Hg(1)-Cl(1)	90.350(148)	N(3)-Hg(1)-Cl(2)	87.698(150)
N(3)-Hg(1)-O(1)	129.601(171)	O(1)-Hg(1)-Cl(1)	91.697(110)
O(1)-Hg(1)-Cl(2)	103.721(114)	C(16)-N(1)-Hg(1)	116.2(4)

Table S5. Fluorescence decay time constants of **L**, **L**-Cd^{2+} and **L**-Hg^{2+}.

	A_1	τ_1/ns	A_2	τ_2/ns	$<\tau>$/ns	χ^2
L at 415 nm	17%	4.952	83%	0.772	1.493	1.073
L-Cd at 415 nm	57%	2.091	43%	10.048	5.506	1.182
L-Hg at 415 nm	91%	0.672	9%	7.258	1.263	1.073

Table S6. The contribution of the orbital transitions to the lowest energy transition of **L**, **L**-Cd^{2+} and **L**-Hg^{2+}.

electronic transition	**L** oscillator strength (f)	electronic transition	**L**-Cd^{2+} oscillator strength (f)	electronic transition	**L**-Hg^{2+} oscillator strength (f)
HOMO–2→LUMO (44%)	0.5442	HOMO–8→LUMO+2 (20%)	0.2336	HOMO–1→LUMO+6 (38%)	0.1678
HOMO→LUMO+2 (28%)	0.5442	HOMO→LUMO+3 (19%)	0.2336	HOMO→LUMO+4 (13%)	0.1678
HOMO–4→LUMO+1 (62%)	0.1707	HOMO–7→LUMO (17%)	0.2336	HOMO–5→LUMO (7%)	0.1678
HOMO–2→LUMO+1 (11%)	0.1707	HOMO–4→LUMO+4 (10%)	0.2336	HOMO–7→LUMO+2 (22%)	0.1677